Available online at www.sciencedirect.com
ScienceDirect
Journal of Catalysis 245 (2007) 25–34
JOURNAL OF CATALYSIS
www.elsevier.com/locate/jcat

Kinetics and reaction pathway of the CO_2 reforming of methane on Rh supported on lanthanum-based solid

John F. Múnera [a], Silvia Irusta [a], Laura M. Cornaglia [a,*], Eduardo A. Lombardo [a], Deborah Vargas Cesar [b], Martin Schmal [b]

[a] *Instituto de Investigaciones en Catálisis y Petroquímica (FIQ, UNL-CONICET), Santiago del Estero 2829-3000 Santa Fe, Argentina*
[b] *NUCAT/PEQ/COPPE, Universidad Federal de Rio de Janeiro, C.P. 68052,21945-0, Rio de Janeiro, Brazil*

Received 25 May 2006; revised 11 September 2006; accepted 11 September 2006

Available online 18 October 2006

Abstract

Rh/La_2O_3 catalysts are very stable for the dry reforming of methane. To understand this catalytic behavior, this system was thoroughly characterized using a battery of instrumental techniques: XRD, LRS, DRIFTS, and XPS. The data obtained with the fresh calcined and reduced solids during reaction and after use, at both the volumetric and surface levels, led to a satisfactory description of the working catalyst that in turn suggested a possible reaction mechanism. It is proposed that the slow steps are both the decomposition of methane ($C + 2H_2$) and the reaction of the carbon species left on the surface with the oxycarbonates present in the working catalyst. The kinetic data obtained by varying the reactant partial pressures between 2.5 and 40 kPa in the temperature range of 823–903 K is well fitted by the kinetic equation derived from the proposed reaction mechanism.

Keywords: CO_2 methane reforming; Kinetics; H_2 production; Rh/La_2O_3

1. Introduction

$Rh(0.6\%)/La_2O_3$ is an excellent catalyst for the dry reforming of methane at temperatures below 600 °C. Using this catalyst, the activity remains unchanged after 150 h on stream; no carbon formation is detected by TGA, and weak Raman bands corresponding to graphitic carbon are observed [1]. This formulation was then selected for use in a Pd membrane reactor to produce ultrapure hydrogen with good success [2].

To model, simulate, and optimize the membrane reactor, a reliable kinetic equation is needed that is not available in the literature. A few papers have been published in which Rh/La_2O_3 catalysts have been used for the dry reforming of methane [3–6]. None of these provide the needed kinetic equation, however Wang and Ruckestein [5] provided some interesting clues about the nature of Rh–La_2O_3 interaction. They found that $LaRhO_3$ is present in the catalyst calcined at 1073 K (XRD). This is consistent with our finding that Rh/La_2O_3 is harder to reduce than Rh/SiO_2 when both are calcined at the same temperature of 873 K [1]. This justifies the stability of the formulations. Another related system, Ru/La_2O_3, studied by Matsui et al. [7], provides data that may be applicable to our system. The XRD patterns of this formulation clearly show the presence of lanthanum oxycarbonate in the used catalysts. Moreover, Verykios and co-workers [8], studying the Ni/La_2O_3 system, detected the presence of $La_2O_2CO_3$ in the used catalysts and assigned a precise role to this compound in the reaction mechanism. They developed a kinetic equation for the dry reforming of methane over Ni/La_2O_3 and reported a fractional order dependency of the rate of reactant disappearance for both P_{CH_4} and P_{CO_2}. In contrast, Wei and Iglesia [9] reported a first-order dependency for P_{CH_4} and zero order for P_{CO_2} when they carried out the reaction on Rh supported on various carriers but not including La_2O_3.

In this work, the catalyst under study was characterized using various instrumental techniques, and the kinetic data were obtained under differential conditions with varying reactant par-

* Corresponding author. Fax +54 342 4571162.
E-mail address: lmcornag@fiqus.unl.edu.ar (L.M. Cornaglia).

0021-9517/$ – see front matter
doi:10.1016/j.jcat.2006.09.008

tial pressures at reaction temperatures of 823–903 K. The goal of this study was to obtain a reliable kinetic equation, consistent with the detailed information provided by the characterization techniques used in this research.

2. Experimental

2.1. Catalyst preparation

The Rh(0.6%)/La_2O_3 catalyst was prepared by conventional wet impregnation of $RhCl_3{\cdot}3H_2O$ onto La_2O_3 (Anedra 99.99%). The impregnated solid was then heated at 353 K to evaporate the water and dried at 383 K overnight. The catalyst was calcined for 6 h at 823 K and then reduced at 823 K in a H_2 flow for 2 h.

2.2. Kinetic measurements

Kinetic studies under differential conditions were conducted in a conventional flow system consisting of a flow measuring and control system, a mixing chamber, and a fixed-bed reactor (5 mm i.d.), which was placed in an electric oven. The feed and product streams were analyzed with a gas chromatograph equipped with a thermal conductivity detector and both Porapak Q and molecular sieve columns. The mass of catalyst used was 10–20 mg. Conversions were usually controlled to be significantly lower than those defined by thermodynamic equilibrium by adjusting the total flow rate (187 ml/min). Rate limitation by external and/or internal mass transfer under differential conditions proved to be negligible by applying suitable experimental criteria.

2.3. Catalyst characterization

2.3.1. Metal dispersion

Rh dispersion of the fresh catalyst after hydrogen reduction at 823 K for 2 h was determined by static equilibrium adsorption of H_2 or CO at room temperature in a conventional vacuum system. The determination of free metal surface area has been reported [10] as a complex issue in lanthanum-based catalysts, where support moieties are thought to decorate the metal surface. In our case, a similar dispersion value was obtained using H_2 or CO chemisorption measurements. The Rh dispersion was equal to 14%.

2.3.2. In situ Diffuse Reflectance Fourier Transform Infrared Spectroscopy (DRIFTS)

Experiments were carried out with a diffuse reflectance infrared cell with ZnSe windows, adapted to a FTIR Nicolet 740 spectrometer. In one set of experiments, the interaction of CO_2 with both the support and the catalyst was studied. In another case, the interaction of the same solid with the reaction mixture was monitored at varying temperatures. In all cases, the sample was loaded into the DRIFTS cell, then heated to 823 K under a flowing H_2/He mixture and kept at this temperature for 2 h. In one experiment, the sample was cooled to 423 K in flowing He, after which the solid was exposed to a flowing stream of 10% CO_2/He mixture to monitor the changes occurring in the IR spectra while increasing the temperature at a rate of 10 K/min up to 923 K. The spectra were taken at different temperatures. After each temperature was reached, it was kept constant for 10 min to stabilize the sample before obtaining the spectrum.

In another experiment designed to analyze the formation of species during the CO_2-reforming reaction, after reduction, the samples were cooled to 773 K in flowing He and then the reaction mixture was fed ($CH_4/CO_2/He = 1/1/18$). The reaction temperature was varied between 773 and 873 K. The spectrum of the sample after the reduction step was used as background.

2.3.3. X-ray photoelectron spectroscopy

The XPS measurements were carried out using a PHI model 1257 electron spectrometer. Nonmonochromatic Al$K\alpha$ X-ray radiation (1486.6 eV) was used. The photoelectron kinetic energy was measured with a hemispheric analyzer in 46.95 eV/step pass energy. The pressure in the analysis chamber was about 1×10^{-7} Pa during spectra collection. The XPS analyses were performed on the used catalyst and on the calcined solids before and after treatment with hydrogen in the reaction chamber attached to the spectrometer. The samples were transferred to the instrument without exposure to air. The spectra from the regions related to La 3d, C 1s, O 1s, and Rh 3d core levels were recorded for each sample.

2.3.4. Laser Raman spectroscopy

The Raman spectra were recorded with a TRS-600-SZ-P Jasco Laser Raman instrument, equipped with a charge-coupled device with the detector cooled to about 153 K using liquid N_2. The excitation source was the 514.5-nm line of a Spectra 9000 Photometrics Ar ion laser. The laser power was set at 30 mW.

3. Results

3.1. Characterization

3.1.1. Laser Raman spectroscopy

Lanthanum oxide carbonates exist in three crystalline modifications: I, Ia, and II. The three polymorphs hold in an arrangement of ($La_2O_2^{2+}$) layers separated by CO_3^{2-} ions. Type I has square layers and is tetragonal, whereas type Ia is described as a monoclinic distortion of form I [11]. II-$La_2O_2CO_3$ is completely indexed in the hexagonal unit cell. The FTIR spectrum of this phase showed bands at 1504, 1467, 1087, 856, and 747 cm^{-1} [12]. A signal at 1368 cm^{-1} and a threefold splitting due to more than one $CO_3^{=}$ type are characteristic of the type Ia phase. A more detailed study of the characterization of the structure of solids supported on lanthanum oxide using LRS, FTIR, and XRD has been described previously [2,11].

The Raman spectra of the Rh/La_2O_3 catalyst after different treatments at 823 K are shown in Fig. 1. All of the solids exhibited peaks at 358, 384, 747, and 1086 cm^{-1}, previously assigned to the hexagonal form of the lanthanum oxycarbonate (II-$La_2O_2CO_3$). The small signals appearing at ca. 1400 cm^{-1} are due to the vibration of $CO_3^{=}$ groups in the type II phase.

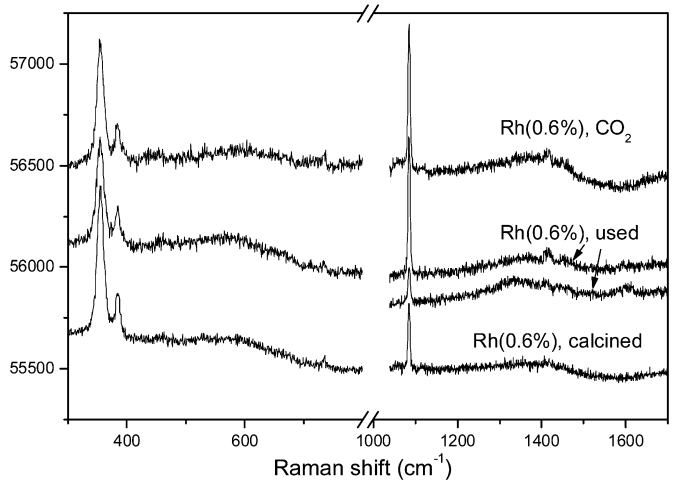

Fig. 1. Laser Raman spectra of the calcined Rh(0.6)/La_2O_3 catalyst and after CO_2 reforming of methane at 823 K.

The XRD pattern (not shown) for the calcined and CO_2-treated solids are in agreement with the Raman spectra.

For the used sample, a group of broad, very-low-intensity Raman bands at 1340 and 1590 cm^{-1} were observed. Both peaks correspond to the presence of small amounts of graphitic carbon.

3.1.2. *In situ DRIFTS analysis*

CO_2 reaction DRIFTS spectra of the La_2O_3 support and the Rh-supported catalyst after reduction at 823 K and CO_2 adsorption at 423 K are shown in Fig. 2. On the support, two well-defined bands at 1310 and 1550 cm^{-1} are observed, whereas a band at 1430 cm^{-1} is seen on the catalyst in the 1300–1600 cm^{-1} range. The bands at 1310–1510 cm^{-1} have been assigned to modes of surface formate species [13]. The observation of additional bands at ca. 2900–2800 cm^{-1} could confirm this assignment. The H source for the formation of formate species could be provided by the surface hydroxyls from the support. However, in the spectra of our samples treated with CO_2 (Fig. 2), no well-defined bands were observed at 2800–2900 cm^{-1}.

Taking into account the above comment, the bands in the 1300–1600 region could be attributed to the $La_2O_2CO_3$. The low-wavenumber band at 1360 cm^{-1} is characteristic of type Ia oxycarbonate observed on the support after CO_2 adsorption at high temperature. The presence of the 1430 cm^{-1} band in the case of the Rh-supported solid could suggest that Rh favors the formation of type II oxycarbonate.

In the high-frequency range (hydroxyl groups), no bands at 3660 cm^{-1}, corresponding to isolated surface terminal La–OH groups [12], were observed. The broad adsorption at approximately 3480 cm^{-1} has been assigned to interacting OH groups [12] or to bridging OH groups [13]. In our samples, this feature decreased with temperature and became a negative band at 823 K. This indicates that the OH groups react with CO_2.

$CO_2 + CH_4$ reaction DRIFTS spectra of the hydrogen-treated support and Rh/La_2O_3 solid after exposure to the reacting mixture at 773–873 K are shown in Fig. 3. In all cases, bands at 720, 842, 864, 1060, and 1550 cm^{-1} assigned to different types of $La_2O_2CO_3$ are observed [11]. Oxycarbonate formation was favored when the reaction temperature was increased, attributed to the reaction between La_2O_3 and CO_2. Simultaneously, the vibration of carbon dioxide in the gas phase decreased with increasing temperature. At the same time, the methane vibration intensity in the gas phase remained constant for the support, whereas the intensity in the catalyst spectra decreased, indicating the overall reaction between methane and CO_2.

The band at 1363 cm^{-1} can be assigned to adsorbed formate species or type Ia oxycarbonate. The appearance of the band at 2860 cm^{-1} confirms formate formation on the Rh/La_2O_3 cata-

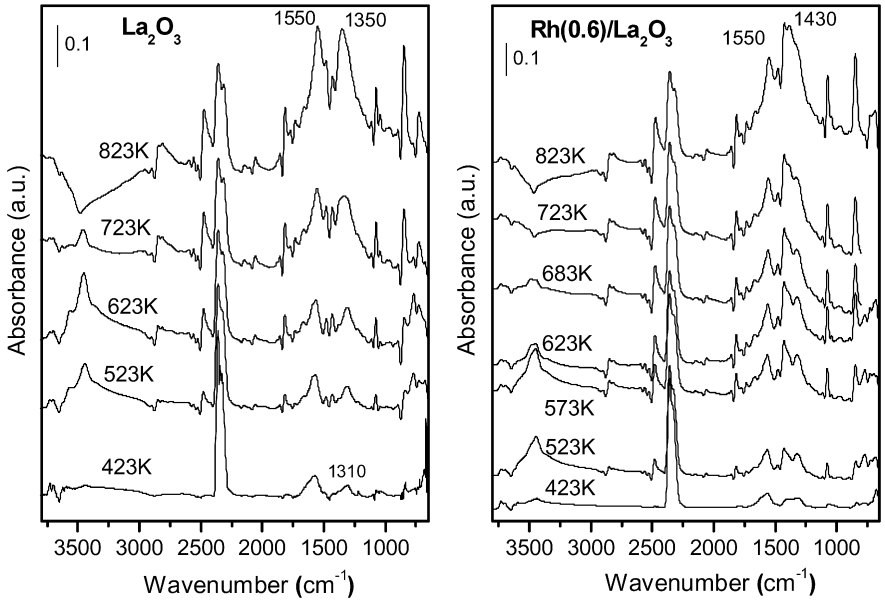

Fig. 2. DRIFT spectra of La_2O_3 and Rh(0.6)/La_2O_3 during exposure to CO_2 at different temperatures, referenced to spectrum of the reduced catalysts prior to gas admission.

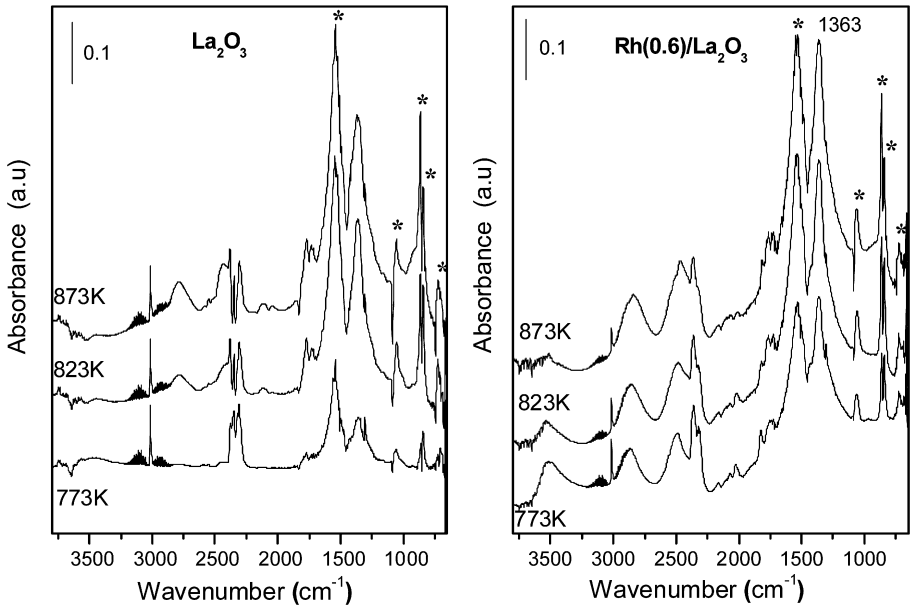

Fig. 3. DRIFT spectra of La_2O_3 and Rh(0.6)/La_2O_3 during exposure to reaction mixture $CO_2 + CH_4 + He$ at different temperatures, referenced to spectrum of the reduced catalysts prior to gas admission.

lyst. The broad OH band at 3500 cm^{-1} disappeared at 873 K. However, splitting of the υ_2 modes in carbonate vibration at approximately 860 and 842 cm^{-1} also suggests the presence of type Ia oxycarbonate.

In the support spectra, a new band at 2770 cm^{-1} appeared at temperatures above 823 K, followed by an increase in the intensity of the band at 1360 cm^{-1} and the presence of the splitting of the υ_2 modes in carbonate vibration. Therefore, both adsorbed formate and type Ia oxycarbonate could be present on the support. The H source for the formate species formation could be provided by the surface hydroxyls from the support. Note that the broad band at approximately 2800 cm^{-1} could represent the contribution of adsorbed CH_x [14] and/or carbonate overtones [11].

In the catalyst spectra, two very-low-intensity features are visible at 1825 and 2036 cm^{-1}. These are assigned to bridge and linearly adsorbed CO on metallic rhodium, respectively.

3.1.3. XPS data

Fig. 4a shows the Rh 3d spectra obtained on the Rh(0.6%)/La_2O_3 after calcination, in situ reduction at 723 K, and CO_2 reforming of methane at 823 K. The intensity ratios and binding energies (BEs) are given in Table 1. BEs were referenced to C 1s = 284.4 eV, resulting in a BE of 834.0 eV for La $3d_{5/2}$ in the rhodium solid. For the calcined solid, the BE of Rh $3d_{5/2}$ was 308.1 eV (Table 1). According to the literature, these high energy values indicate the presence of Rh^{n+} species. BE values for Rh^+ compounds of 307.6–309.6 eV have been reported by Nefedov et al. [15]; others [16] have reported BEs for Rh^{2+} compounds within a similar range (308.4–309.3 eV). The Rh^{3+} oxidation state has a BE of 309.7 eV [17]. In the case of pure Rh metal foil, a Rh $3d_{5/2}$ peak occurs at 307.0 eV, with 1.6 eV FWHM [18].

Regarding the spectra in Fig. 4a, the Rh $3d_{3/2}$ and Rh $3d_{5/2}$ peaks exhibited a shift to lower BEs on reduction, indicating reduction to Rh^0 compared with that in the calcined sample. For the calcined solid, the broad peak (FWHM = 3.1 eV) suggests the presence of Rh^{3+} and Rh^+ surface species. On the other hand, the used catalyst had a Rh 3d BE even lower than that of the reduced sample.

The FWHM of Rh $3d_{5/2}$ peak mainly reflects the particle size [10,19,20]. The increased FWHM for small particles, where the BE is also sensitively size-dependent, originates from the particle size distribution. The used catalyst had a greater FWHM than the reduced Rh; the BE was 0.9 eV higher for the former than for the used solid. This indicates smaller average particle size and broader size distribution in the reduced solid; however, the small difference is not significant. For the reduced catalyst, the Rh/La atomic ratio was slightly decreased compared with that of the calcined and used sample during reaction in an integral reactor, suggesting that no change in the rhodium dispersion occurred.

The C 1s spectra show only two well-defined peaks at 284.4 and 289.2 eV. The low-BE peak corresponds to the contamination carbon. This BE changed to 283.6 eV for the used solid due to the presence of low amounts of graphitic carbon, as detected by laser Raman spectroscopy. The peak at 289.1 ± 0.2 eV can be attributed to carbonate carbon [10], consistent with the presence of the O 1s peak at 530.1 eV (Figs. 4b and 4c) assigned to the same species. After reduction, the intensity of carbonate signal decreased (Table 1), and a contribution at 527.7 eV appeared in the O 1s region, which is assigned to lattice oxygen $O^=$ [12].

XPS spectra in the O 1s region were fitted to analyze the contribution of both oxygen species, assigning BEs of 527.7 eV to the lattice oxygen and 530.1 eV to the oxygen of the carbonate species [10]. The results of the spectrum adjustment are displayed in Table 1. For the calcined sample, the major contribution was the carbonate oxygen; the intensity of this higher

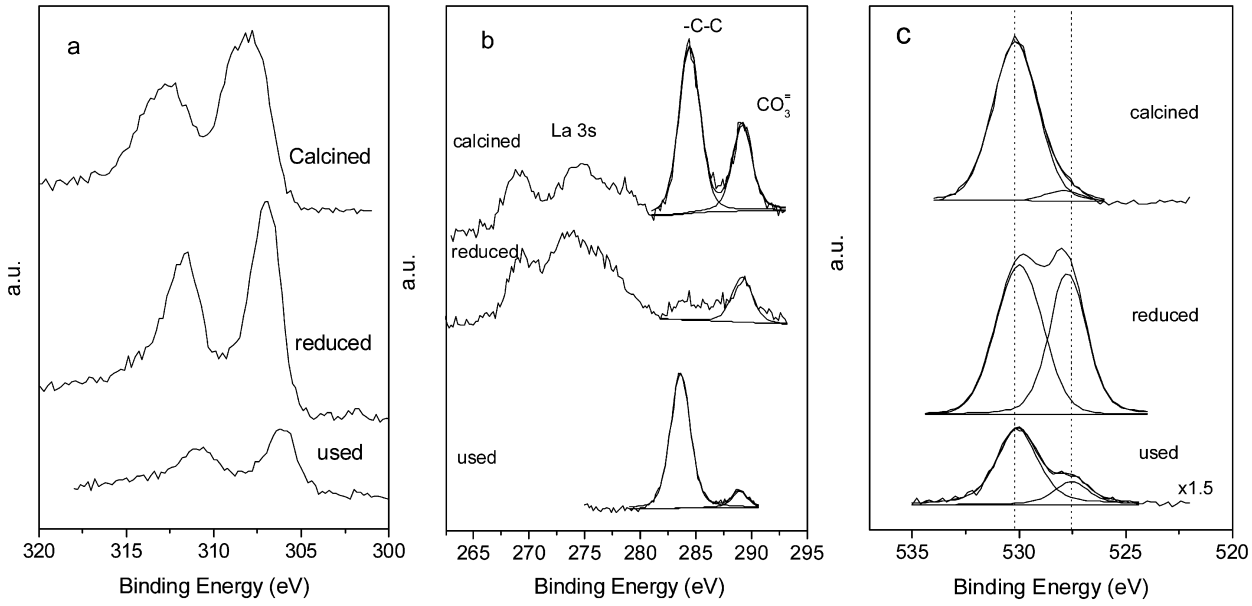

Fig. 4. (a) Rh 3d, (b) O 1s and (c) C 1s XPS from Rh(0.6)/La_2O_3 solid: calcined, after hydrogen reduction and used in a fixed-bed reactor.

Table 1
Binding energies[a] and surface atomic ratio for Rh(0.6%)/La_2O_3

Solid	C 1s $CO_3^=$ (eV)	Rh $3d_{5/2}$ (eV)	O 1s (eV)	$CCO_3^=$/La	Rh/La	O/La	$C_{CO_3^=}/O_{CO_3^=}$
Calcined	289.2	308.1 (3.1)[b]	530.1(90%)[c] 528.0(10%)	1.6	0.46	1.6	1.0
H_2, in situ at 450 °C	289.3	307.0 (1.8)	530.1(50%) 527.8(50%)	0.65	0.30	2.0	0.65
Used	288.9	306.1 (2.0)	530.1(80%) 527.5(20%)	0.87	0.41	2.3	0.50

[a] Contamination carbon was taken as reference at 284.4 eV.
[b] FWHM are given between parenthesis.
[c] O 1s peak relative intensity.

BE peak was 90% of the total signal, whereas in the reduced solid, the two peaks were in similar proportions. For the catalyst used in the integral reactor, the carbonate O 1s peak represented 80% of the total signal intensity. The $C_{CO_3^=}/O_{CO_3^=}$ atomic ratios decreased for the used sample, suggesting that oxycarbonate formation occurred.

3.2. Kinetic measurements

The influence of the partial pressure of reactants on the rate of methane consumption is depicted in Figs. 5a and 5b. These studies were performed at atmospheric pressure in the temperature range of 823–903 K under differential conditions. The measurements were made maintaining the partial pressure of one reactant constant (10 or 40 kPa) and varying the other reactant pressure between 2.5 and 40 kPa. The four plots shown in Figs. 5a and 5b have similar shapes, although in terms of the rates obtained at low pressure of either reactant, P_{CH_4} has a stronger influence than P_{CO_2} on r_{CH_4}. This is symptomatic of a lower reaction order for CO_2 than for CH_4.

Using $\ln r$ versus $\ln P$ plots is useful for estimating the reaction orders with respect to both reactants. It is more rigorous to plot the log of the rate of the forward reaction (r_f) versus either $\ln P_{CH_4}$ or $\ln P_{CO_2}$ to substantiate this matter. Calculating r_f from the net rate of reaction (r_n) can be done as follows:

$$r_f = r_n(1-\eta), \tag{1}$$

$$\eta = \frac{(P_{CO})^2}{P_{CH_4}} \frac{(P_{H_2})^2}{P_{CO_2}} \frac{1}{Ke}, \tag{2}$$

where P_i are the prevalent pressures of reactants and products and Ke is the equilibrium constant calculated at the corresponding reaction temperature. Values of η range from 0.02 to 0.25 for data reported here. Fig. 6 shows the order plots obtained using r_f measured at 823 K. From the slopes of the two straight lines, the resulting power law rate equation is

$$r_{f(CH_4)} = k(P_{CH_4})^{0.61}(P_{CO_2})^{0.37}. \tag{3}$$

If the r_n values are used instead, then the reaction orders are somewhat lower: 0.51 and 0.24, respectively. The results reported in Figs. 5 and 6 indicate that CO_2 is more strongly adsorbed than CH_4 on La_2O_3. This is consistent with the strong CO_2–La_2O_3 interaction revealed by the formation of oxycarbonates that were detected through both XRD and IR spectroscopy in the used catalyst [11].

The effect of the hydrogen partial pressure upon the rate of disappearance of both reactants and the rate of formation

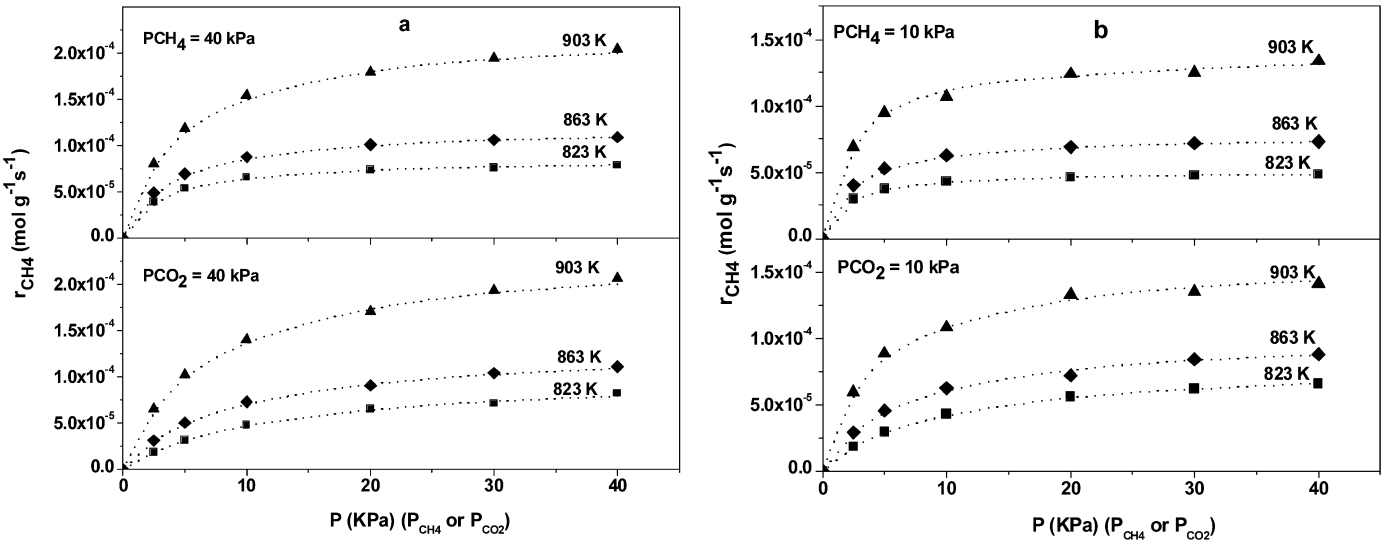

Fig. 5. Dependence of the rate of CH_4 on methane partial pressure and carbon dioxide partial pressure at 823, 863 and 903 K. Reaction conditions: Total pressure = 100 kPa. (a) Constant partial pressure = 40 kPa. (b) Constant partial pressure = 10 kPa.

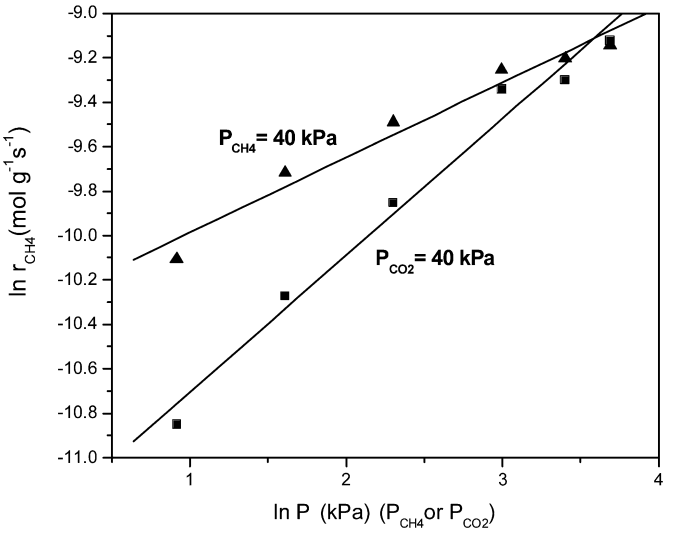

Fig. 6. Order plots obtained using methane forward rates measured at 823 K.

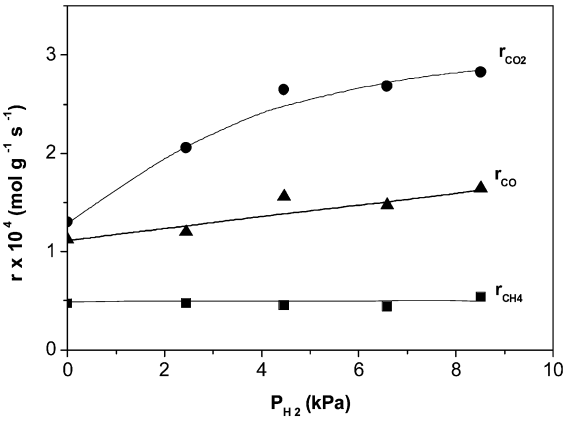

Fig. 7. Effect of hydrogen partial pressure on the rate of methane and carbon dioxide consumption and CO production at 823 K.

of CO may reveal important details of the reacting system. Fig. 7 shows that r_{CH_4} is not affected by P_{H_2}. This means that the $CO_2 + CH_4$ reaction is far from equilibrium. Note, however, that this is not the case when supported nickel is used as catalyst; Bradford and Vannice [21] reported the formation of methane on increasing P_{H_2}. This is consistent with the fact that supported nickel is a good methanation catalyst, much better than rhodium.

In contrast, increasing P_{H_2} increases both the carbon monoxide formation (r_{CO}) and the CO_2 consumption (r_{CO_2}) rates (Fig. 7). This is symptomatic of the role played by the reverse water–gas shift reaction (RWGS). Furthermore, the H_2/CO ratio is much lower than unity, the value expected from the $CO_2 + CH_4$ stoichiometry. Fig. 8 shows the evolution of both the experimental and equilibrium H_2/CO ratios with reaction temperature. The latter ratio was calculated using the thermodynamic data for both dry reforming and the RWGS. The similar evolution of H_2/CO equilibrium and experimental ratios with temperature is also consistent with the parallel RWGS occurring at a faster rate than the dry reforming of methane. Fig. 9 further confirms that the RWGS occurs so fast on Rh/La_2O_3 that it is essentially equilibrated with all of the reaction temperatures explored in this work.

3.3. Apparent activation energies

To compare our data with other data published in the literature, the apparent activation energies were calculated from Arrhenius-type plots for the turnover frequencies (TOFs) of reactants and products (Fig. 10). These TOFs were calculated by normalizing the reaction rates to the number of exposed surface Rh atoms. The Rh dispersion measured by either H_2 or CO chemisorption was similar and equal to 14%. The activation energies calculated from the slopes of these plots are shown in Table 2 and compared with similar data reported in the litera-

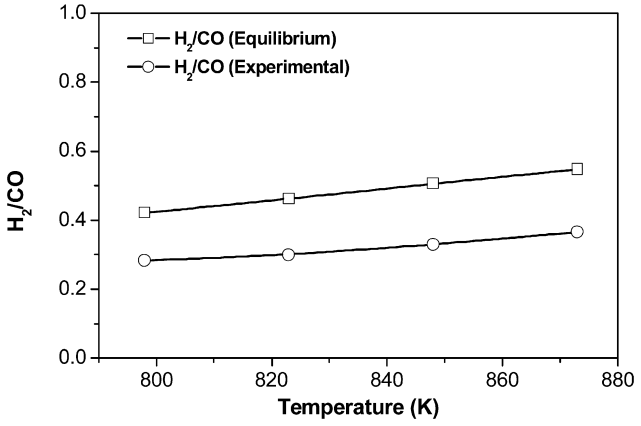

Fig. 8. H_2/CO product ratio as a function of temperature. Reaction conditions: Total pressure = 100 kPa, $CO_2/CH_4/He = 1/1/1$.

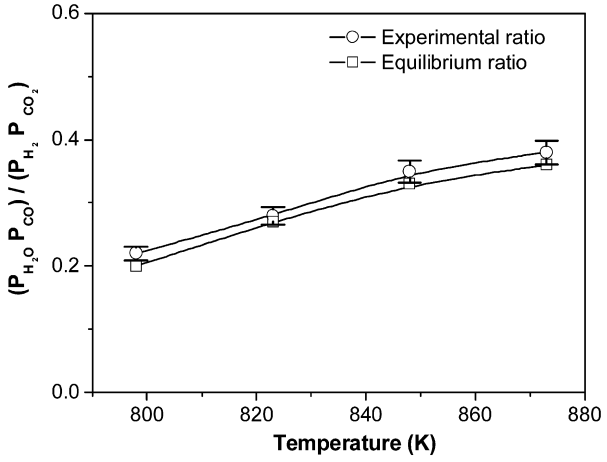

Fig. 9. Experimental reverse water gas shift pressure ratios compared to theoretical equilibrium ratio. Reaction conditions: Total pressure = 100 kPa, $CO_2/CH_4/He = 1/1/1$.

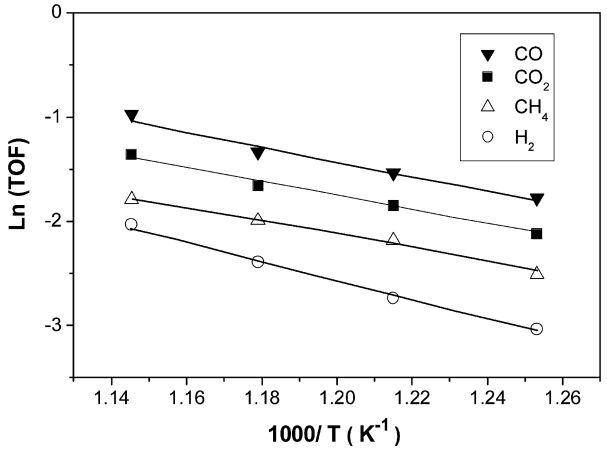

Fig. 10. Arrhenius plots of turnover frequencies on Rh(0.6)/La_2O_3. Reaction conditions: Total pressure = 100 kPa, $CO_2/CH_4/He = 1/1/1$.

ture. In our case, the activation energies for the disappearance of CH_4 and CO_2 were very close to and lower than other values reported in the literature. The activation energy for the formation of H_2 was ca. 4.8 kcal/mol higher than the activation energy for the formation of CO. This could be related to the parallel occurrence of the RWGS, which consumes H_2 and produces CO. Note that all of the data collected in Table 2 show differences in activation energies in the same direction, but these vary between 0.8 [24] and 11.5 [21], although most differ by only 2–4 kcal/mol (Table 2). These temperature dependencies will be taken up again in reference to the kinetic model introduced in the next section.

Table 2
Apparent activation energies

Catalyst	Activation energies[a]				Ref.
	E_{ap} (kcal/mol)				
	r_{CH_4}	r_{CO_2}	r_{CO}	r_{H_2}	
Rh(0.6%)/La_2O_3	12.74	13.04	14.18	18.94	This work
Rh(1.0%)/Al_2O_3	–	–	16.00	18.00	[22]
Rh (1.0%)/MgO	–	–	20.00	23.00	[22]
Rh (1.0%)/TiO_2	–	–	12.00	16.00	[22]
Rh(3.8%)/SiO_2	19.00	21.73	20.77	23.40	[27]
Pt(0.83%)/ZrO_2	18.40	15.00	15.00	16.80	[24]
Pt(0.86%)/Al_2O_3	22.50	20.20	18.50	19.30	[24]
Pt(0.31%)/ZrO_2	24.00	20.00	21.60	34.00	[21]
Pt(0.82%)/TiO_2	23.00	19.00	20.50	32.00	[21]
Pt(0.75%)/Cr_2O_3	16.00	15.00	16.00	19.00	[21]

[a] Calculated from the graph: ln(TOF) vs T^{-1}.

4. Discussion

4.1. Oxycarbonate formation

To obtain more information about the interaction of these catalysts with the reactants, DRIFTS spectra were obtained after CO_2 adsorption as well as during the dry reforming of methane. The behavior of the Rh/La_2O_3 compared with the support when exposed to CO_2 at high temperatures indicated that Rh favored type II oxycarbonate formation. However, when the catalyst was exposed to a mixture of CO_2 and CH_4, adsorbed formate species and type Ia oxycarbonate were present. This explanation is supported by the appearance of the bands at 1360 and 2860 cm^{-1} and the splitting of the υ_2 modes (860 and 842 cm^{-1}) in carbonate vibration. These observations are consistent with those in a previous report [13] in that the oxycarbonate formation on Ni/La_2O_3 was observed. However, they do not distinguish between the different oxycarbonate types.

Most of the DRIFTS studies of Rh supported on other systems (Al_2O_3, ZrO_2, and SiO_2) [26–28] have reported the formation of linear and bridged CO on metallic Rh as the dominant surface species under reaction conditions. At high temperatures, formate species have been detected in the same cases.

Our DRIFTS findings are in agreement with the XPS results. In our used Rh catalyst, the $C_{CO_3^=}/O_{CO_3^=}$ XPS atomic ratio decreased compared with the calcined and reduced solid, and the surface ratio was close to the stoichiometric value for $La_2O_2CO_3$. Through XPS analysis, Verykios [13] reported the presence of a substantial carbon overlayer on the reduced Ni/La_2O_3 catalyst consisting of –C–C, –O–C, and $CO_3^=$ species. After exposure to reactants, they found that –COO– species were generated.

4.2. Reaction mechanism

Of the numerous publications concerning the CO_2 reforming of methane, in what follows we review those more directly connected with Rh/La_2O_3. Rhodium has been supported on many oxides and even in a few cases on La_2O_3 [3–6]. In the latter case, not very much has been said about the reaction mechanism. Wei and Iglesia [9], in a very thorough mechanistic-kinetic study of this reacting system over Rh/Al_2O_3, determined that $r_{CH_4} = kP_{CH_4}$. This could be due to the low adsorption of CO_2 on alumina compared to what we found on Rh/La_2O_3 [Fig. 6; Eq. (3)].

Lanthanum oxide has been used as support for other metals besides Rh, including Ni, Ru, and Ir. In particular, the studies on Ni/La_2O_3 and Ru/La_2O_3 catalysts provide interesting backup information for our system. Matsui et al. [7] investigated the reaction mechanism of the $CO_2 + CH_4$ reaction over Ru/Al_2O_3 and Ru/La_2O_3. They confirmed that the alumina adsorbed very little CO_2, whereas La_2O_3 rapidly formed $La_2O_3CO_3$. According to these authors, these species contribute to methane activation and the consequent dissociation of CH_x over the metal clusters. The broad band observed in our DRIFTS spectra at approximately 2800 cm^{-1} could include the contribution of adsorbed CH_x and/or formate species [14]. Recently, rigorous studies [9] have proposed that CH_4 irreversibly decomposes in a sequence of elementary steps to form chemisorbed carbon and hydrogen atoms and have claimed the kinetic relevance of C–H bond activation steps.

On the other hand, the work of Tsipouriari and Verykios [8] provides much insight concerning the reaction mechanism and kinetic behavior of dry reforming of methane over Ni/La_2O_3. These authors concluded that the formation of oxycarbonates during reaction plays a central role in the dry reforming of methane. Through steady-state isotopic tracing kinetic analysis, they found that methane exists on the catalyst surface under reaction conditions [23]. The CH_4 decomposes on the nickel crystallites to yield H_2 and adsorbed carbon that reacts with the oxycarbonate at the metal–support interface to liberate CO and at the same time clean up the metallic surface.

Based on the foregoing, we report a number of observations derived from our characterization results that lead us to propose the following reaction mechanism for our Rh–lanthanum-based system, which resembles that proposed by Verykios and coworkers for Ni/La_2O_3:

1. The presence of $La_2O_2CO_3$ in Rh/La_2O_3 was detected through XRD, FTIR and Raman spectroscopy [1,2]. The strong CO_2-support interaction is consistent with the lower order for this reactant than for H_2 (Fig. 6). Furthermore, the DRIFTS spectra obtained during reaction (Fig. 3) clearly indicate the presence of the less stable, more reactive type Ia oxycarbonate.
2. No carbon deposition could be detected through TGA, whereas weak Raman bands of graphitic carbon were observed in used catalysts. No deactivation was observed after 180 h on stream [1,2], suggesting that the graphitic carbon was not formed on the Rh surface.
3. The constancy of r_{CH_4} with hydrogen pressure (Fig. 7) is consistent with the observations made by others [7,25,29] that the cracking of methane adsorbed on the metal (Ni, Ru, Rh) is a slow reaction step.
   In view of these observations, the main reactions occurring when CO_2 and CH_4 adsorb on Rh/La_2O_3 are likely to be:

$$CH_4 + S \overset{K_1}{\longleftrightarrow} S\text{–}CH_4 \quad \text{(equilibrium)}, \tag{4}$$

$$S\text{–}CH_4 \xrightarrow{k_2} S\text{–}C + 2H_2 \quad \text{(slow step)}, \tag{5}$$

$$CO_2 + La_2O_3 \overset{K_3}{\longleftrightarrow} La_2O_2CO_3 \quad \text{(equilibrium)}, \tag{6}$$

$$La_2O_2CO_3 + C\text{–}S \xrightarrow{k_4} La_2O_3 + 2CO + S \quad \text{(slow step)}. \tag{7}$$

   The mechanistic picture is that methane reversibly adsorbs on the metallic clusters [Eq. (4)] while the cracking of the adsorbed species proceeds, slowly liberating H_2 and generating carbon that remains on the metallic surface. The CO_2 rapidly reacts with La_2O_3 to generate oxycarbonate, which in turn reacts slowly with carbon [Eq. (7)] to generate the other main product, CO. This slow reaction occurs most likely at the metal/support interface. Note that the RWGS occurs simultaneously all of the time and is always equilibrated (Fig. 9).
   In the other hand, step 5 could be substituted for a series of elementary H-abstraction steps that can be written as:

$$S\text{–}CH_4 \xrightarrow{k_2} S\text{–}CH_x + \frac{(4-x)}{2}H_2 \quad (0 \leqslant x \leqslant 4). \tag{5a}$$

4.3. Kinetic modeling

The rate equation that fits our data has been derived assuming that Eqs. (5) and (7) represent the rate-determining steps and that the surface coverage of H_2 and CO adsorbed are negligible. Considering step (5a) the same rate expression can be obtained.

$$r_{CH_4} = \frac{K_1 k_2 K_3 k_4 [CH_4][CO_2]}{K_1 K_3 k_4 [CH_4][CO_2] + K_1 k_2 [CH_4] + K_3 k_4 [CO_2]}. \tag{8}$$

Using Eq. (8), our data were fitted properly, as shown in Fig. 11.

The constant values and the 95% confidence intervals are summarized in Table 3. The temperature dependence of the k_i and K_i were calculated from the raw data obtained between 823 and 903 K,

$$K_1 = 14.0 \times \exp(-3930/T) \quad [\text{kPa}]^{-1}, \tag{9}$$

$$k_2 = 2.44 \times \exp(-8549/T) \quad [\text{mol/g s}], \tag{10}$$

$$K_3 k_4 = 0.012 \times \exp(-4990/T) \quad [(\text{mol/g s})(\text{kPa}^{-1})], \tag{11}$$

and

$$k_4 = 2.47 \times 10^5 \times \exp(-20718/T) \quad [\text{mol/g s}], \tag{12}$$

where K_1 is the equilibrium constant of methane adsorption and k_2 is the rate constant of the decomposition (cracking) of methane on the Rh surface. Using Eq. (8), these two constants

were determined from the slope and interception in the graphic $1/r_{CH_4}$ versus $1/P_{CH_4}$ (not shown). The value 24.8 Kcal/mol [Eqs. (9) and (10)] represents the sum of activation energy of methane cracking and the enthalpy of methane adsorption on Rh.

K_3 is the equilibrium constant of reaction (6), and k_4 represents the kinetic constant of reaction (7). These two constants could not be determined individually from experimental data. The K_3k_4 product was calculated from the slope in the graphic $1/r_{CH_4}$ versus $1/P_{CO_2}$. To calculate the k_4 rate constant, the equilibrium constant for the oxycarbonate formation (K_3) was obtained from data published by Shirsat et al. [30].

The methane adsorption energy exhibits a positive value (7.8 Kcal/mol) and does not satisfy the condition of $-\Delta H > 0$. For the adsorption of CH_4 on metal surfaces, it has been reported [31] that the adsorption energies involved are small, with magnitudes below 0.2 eV (4.5 Kcal/mol). The on-top site was more favorable for the adsorption of methane. From the theoretical calculation on Rh metal surface, Au et al. [31] obtained negative and positive values depending on the site model.

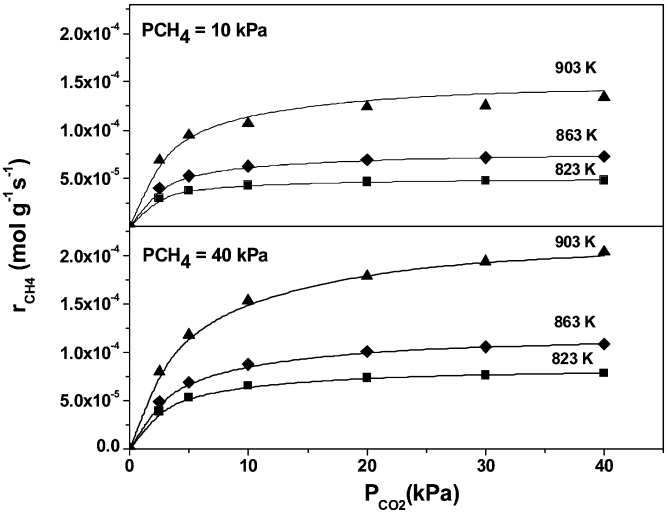

Fig. 11. Fit of the proposed kinetic model for CO_2 reforming of methane as a function of methane and carbon dioxide partial pressures. Curves were calculated using Eq. (8).

These results can explain the positive energy obtained from our kinetic results. However, it should be considered that the low-adsorption energy could lead to the determination of unrealistic values. Although it is possible to retrieve K_1k_2 values from published data obtained with both Pt and Ni supported on several oxides, these data afford little comparison with ours due to the different nature of the active metals and supports. The best reference data were reported by Wei and Iglesia [9], who obtained an activation energy of 26.6 kcal/mol for methane disappearance using Rh(0.4%)/Al_2O_3 as the catalyst. This is very close to our value of 24.8 kcal/mol obtained by adding the values derived from Eqs. (9) and (10). Note that on Al_2O_3 the adsorption of CO_2 is negligible, and, consequently, these authors found a first-order dependency of the reaction rate on methane partial pressure and zero order on carbon dioxide. Other authors who studied the dry reforming of methane on Rh(0.6–1.0%)/Al_2O_3 reported activation energies of 21.0–24.2 kcal/mol [3,32,33].

5. Conclusion

A combination of XRD, LRS, XPS, and DRIFTS techniques revealed that the calcined Rh/La_2O_3 solid after reduction is made up of a mixture of La_2O_3 and oxycarbonates on which reduced dispersed rhodium clusters are sitting. The XPS data of the used catalyst further indicate that the only visible surface species are lanthanum oxycarbonate and mainly Rh°. The DRIFTS data obtained during reaction of $CO_2 + CH_4$ showed the presence of both Ia- and II-$La_2O_2CO_3$, as well as both linear and bridge-bonded CO adsorbed on metallic rhodium. These observations support a reaction mechanism in which the slow steps are the methane decomposition shown in Eq. (5) and the surface reaction of the lanthanum oxycarbonate with the carbon residues left on the surface upon methane decomposition, shown in Eq. (7). Note that this reaction provides a rationale for the stability of this catalyst. The kinetic equation emerging from this mechanism is able to model the catalytic data collected at 823–903 K, with reactant partial pressures varying between 10 and 40 kPa (total pressure, 100 kPa). The activation energy of the combination of Eqs. (4) and (5) is very close to the values reported for Rh supported on other oxides.

Table 3
Kinetic model parameters

Parameters	Temperatures		
	823 K	863 K	903 K
K_1[a,b]	$(86 \pm 4.5) \times 10^{-3}$	$(115 \pm 4.9) \times 10^{-3}$	$(137 \pm 7.1) \times 10^{-3}$
k_2[a,c]	$(1.09 \pm 0.06) \times 10^{-4}$	$(1.44 \pm 0.06) \times 10^{-4}$	$(2.63 \pm 0.14) \times 10^{-4}$
K_3k_4[a,d]	$(2.95 \pm 0.05) \times 10^{-5}$	$(3.34 \pm 0.01) \times 10^{-5}$	$(5.06 \pm 0.06) \times 10^{-5}$
K_3[e]	10.02 ± 0.11	3.74 ± 0.02	1.85 ± 0.003
k_4	$(2.94 \pm 0.03) \times 10^{-6}$	$(8.93 \pm 0.04) \times 10^{-6}$	$(2.74 \pm 0.004) \times 10^{-5}$

[a] Values are reported ±95% confidence interval.
[b] Equilibrium constant of methane adsorption $[kPa]^{-1}$.
[c] Rate constant of the decomposition of methane [mol/g s].
[d] Product of the equilibrium constant of the reaction between CO_2 and La_2O_3 and the rate constant of reaction between the oxycarbonate species and carbon deposited on surface of Rh [(mol/g s)(kPa^{-1})].
[e] From Shirsat et al. [30] $[kPa]^{-1}$.

Acknowledgments

Financial support was provided by UNL, CONICET, and ANPCyT. The authors thank Elsa Grimaldi for the English language editing.

References

[1] S. Irusta, L. Cornaglia, E. Lombardo, J. Catal. 210 (2002) 7.
[2] L. Cornaglia, J. Múnera, S. Irusta, E. Lombardo, Appl. Catal. 263 (2004) 91.
[3] Z.L. Zhang, V.A. Tsipouriari, A.M. Efstathiou, X.E. Verykios, J. Catal. 158 (1996) 51.
[4] L. Basini, D. Sanfilippo, J. Catal. 157 (1995) 162.
[5] H.Y. Wang, E. Ruckenstein, Appl. Catal. 204 (2000) 143.
[6] P. Gronchi, P. Centola, R. Del Rosso, Appl. Catal. A 152 (1997) 87.
[7] N. Matsui, K. Anzai, N. Akamatsu, K. Nakagawa, N. Ikenaga, T. Suzuki, Appl. Catal. 179 (1999) 247.
[8] V. Tsipouriari, X.E. Verykios, Catal. Today 64 (2001) 83.
[9] J. Wei, E. Iglesia, J. Catal. 225 (2004) 116.
[10] G. Gallaher, J. Goodwin, C. Huang, M. Houalla, J. Catal. 140 (1993) 453.
[11] S. Irusta, L. Cornaglia, E. Lombardo, Mater. Chem. Phys. 86 (2004) 440.
[12] S. Lacombe, C. Geantet, C. Mirodatos, J. Catal. 151 (1994) 439.
[13] X.E. Verykios, Int. J. Hydrogen Energy 28 (2003) 1045.
[14] J. Raskó, F. Solymosi, Catal. Lett. 46 (1997) 153.
[15] V.I. Nefedov, E.F. Shubochikina, I.S. Kolomnikov, I.B. Baranovskii, V.P. Golubnichaya, L.K. Chubochkin, M.A. Porai-Koshits, M.E. Vol'pin, Russ. J. Inorg. Chem. 18 (1973) 444.
[16] H. Gysling, J. Monnier, G. Apai, J. Catal. 103 (1987) 407.
[17] T. Lopez, A. Lopez-Gaona, R. Gomez, Langmuir 6 (1990) 1343.
[18] M. Kawai, M. Uda, M. Ichikawa, J. Phys. Chem. 89 (1985) 1654.
[19] S. Zafeirotos, V. Nehasil, S. Ladas, Surf. Sci. 433–435 (1999) 612.
[20] S. Labich, E. Taglauer , H. Knozinger, Top. Catal. 14 (2001) 153.
[21] M.C. Bradford, M.A. Vannice, Appl. Catal. 142 (1996) 97.
[22] A. Erdohely, J. Cserenyi, F. Solymosi, J. Catal. 141 (1993) 287.
[23] V.A. Tsipouriari, X.E. Verykios, J. Catal. 187 (1999) 85.
[24] M. Souza, D. Aranda, M. Schmal, J. Catal. 204 (2001) 498.
[25] M. Bradford, M. Vannice, J. Catal. 173 (1998) 157.
[26] P. Ferreira-Aparicio, M. Férnandez-García, A. Guerrero-Ruiz, I. Rodriguez-Ramos, J. Catal. 190 (2000) 296.
[27] M. Sigl, M. Bradford, H. Knozinger, M.A. Vannice, Top. Catal. 8 (1999) 211.
[28] M. Bradford, M.A. Vannice, Catal. Today 50 (1999) 87.
[29] Z.L. Zhang, X.E. Verykios, Catal. Lett. 38 (1996) 175.
[30] A.N. Shirsat, M. Ali, K.N. Kaimal, S.R. Bharadwaj, D. Das, Thermochim. Acta 399 (2003) 167.
[31] C. Tong Au, C. Fai Ng, M. Sheng Liao, J. Catal. 185 (1999) 12.
[32] J.T. Richardson, S.A. Paripatyadar, Appl. Catal. 61 (1990) 293.
[33] J. Nakamura, K. Aikawa, K. Sato, T. Uchijima, Catal. Lett. 25 (1994) 265.